GEOPHYSICS, VOL. 89, NO. 2 (MARCH-APRIL 2024); P. D131–D138, 12 FIGS.
10.1190/GEO2023-0078.1

Detecting fractures and monitoring hydraulic fracturing processes at the first EGS Collab testbed using borehole DAS ambient noise

David Li[1], Lianjie Huang[1], Yingcai Zheng[2], Yingping Li[3], Martin Schoenball[4], Verónica Rodriguez-Tribaldos[5], Jonathan Ajo-Franklin[6], Chet Hopp[4], Tim Johnson[7], Hunter Knox[7], Doug Blankenship[8], Patrick Dobson[4], Tim Kneafsey[4], and Michelle Robertson[4]

ABSTRACT

Enhanced geothermal systems (EGS) require cost-effective monitoring of fracture networks. We validate the capability of using borehole distributed acoustic sensing (DAS) ambient noise for fracture monitoring using core photos and core logs. The EGS Collab project has conducted 10 m scale field experiments of hydraulic fracture stimulation using 50–60 m deep experimental wells at the Sanford Underground Research Facility (SURF) in Lead, South Dakota. The first EGS Collab testbed is located at 1616.67 m (4850 ft) depth at SURF and consists of one injection well, one production well, and six monitoring wells. All wells are drilled subhorizontally from an access tunnel called a drift. The project uses a single continuous fiber-optic cable installed sequentially in the six monitoring wells to record DAS data for monitoring hydraulic fracturing during stimulation. We analyze 60 s time records of the borehole DAS ambient noise data and compute the noise root-mean-square (rms) amplitude on each channel (points along the fiber cable) to obtain DAS ambient noise rms amplitude depth profiles along the monitoring wellbore. Our noise rms amplitude profiles indicate amplitude peaks at distinct depths. We compare the DAS noise rms amplitude profiles with borehole core photos and core logs and find that the DAS noise rms amplitude peaks correspond to the locations of fractures or lithologic changes indicated in the core photos or core logs. We then compute the hourly DAS noise rms amplitude profiles in two monitoring wells during three stimulation cycles in 72 h and find that the DAS noise rms amplitude profiles vary with time, indicating the fracture opening/growth or closing during the hydraulic stimulation. Our results demonstrate that borehole DAS passive ambient noise can be used to detect fractures and monitor fracturing processes in EGS reservoirs.

INTRODUCTION

There is enormous untapped potential for geothermal electricity generation in the U.S. It is estimated that geothermal electricity generation will grow 26-fold and reach 60 GW by 2050, which is 8.5% of the total U.S. electricity consumption (Lambert, 2022). In an enhanced geothermal system (EGS), we first create fractures in the low-permeability hot rock, such as granite. We then

Manuscript received by the Editor 1 February 2023; revised manuscript received 14 September 2023; published ahead of production 30 November 2023; published online 30 January 2024.
[1]Los Alamos National Laboratory, Los Alamos, New Mexico, USA. E-mail: davidzli@lanl.gov (corresponding author); ljh@lanl.gov (corresponding author).
[2]University of Houston, Department of Earth and Atmospheric Sciences, Houston, Texas, USA. E-mail: yzheng24@central.uh.edu.
[3]University of Houston, Department of Earth and Atmospheric Sciences, Houston, Texas, USA and BlueSkyDAS LLC, Sugar Land, Texas, USA. E-mail: y1p2li58@gmail.com.
[4]Lawrence Berkeley National Lab, Berkeley, California, USA. E-mail: schoenball@lbl.gov; chopp@lbl.gov; pfdobson@lbl.gov; tjkneafsey@lbl.gov; mcrobertson@lbl.gov.
[5]GFZ German Research Center for Geosciences, Albert-Einstein-Straße 42-46, 14473 Potsdam, Germany, and Lawrence Berkeley National Lab, Berkeley, California, USA. E-mail: verort@gfz-potsdam.de.
[6]Rice University, Earth, Environmental and Planetary Sciences, Houston, Texas, USA. E-mail: ja62@rice.edu.
[7]Pacific Northwest National Laboratory, Richland, Washington, USA. E-mail: tj@pnnl.gov; hunter.knox@pnnl.gov.
[8]Sandia National Laboratories, Albuquerque, New Mexico, USA. E-mail: dablank@sandia.gov.

DOI:10.1190/geo2023-0078.1

pump fluid into the geothermal reservoir through an injection well. The injected fluid flows through the fractures created in the reservoir rock while heating up and reaches a production well where the heated fluid/steam is used to turn a turbine to generate electricity. Therefore, reliably monitoring the fracture process in a high-temperature, high-pressure reservoir is crucial for the development of EGS. However, the high-temperature and high-pressure environment of EGS is hostile for conventional electronic seismic instruments that might not be able to survive long-duration deployment for the purpose of continuous monitoring. In contrast, distributed acoustic sensing (DAS) systems using optical fiber cables as receivers would be able to continuously operate in high-temperature, high-pressure environments. Therefore, DAS has become an appealing continuous monitoring tool for EGS (Li et al., 2021).

The EGS Collab project is an interdisciplinary collaborative project among the U.S. Department of Energy's National Labs, academia, and industry to conduct 10 m-scale field experiments of fracture stimulation for EGS modeling analysis and validation (Dobson et al., 2017; Kneafsey et al., 2018; Kneafsey et al., 2019, 2020). The first EGS Collab testbed is located at the 1616.67 m (4850 ft) depth level at the Sanford Underground Research Facility (SURF) in Lead, South Dakota. In the first testbed, the project uses heavily instrumented 50–60 m monitoring wells to study hydraulic fracturing processes using microseismic monitoring (Chen et al., 2019; Fu et al., 2021), hydraulic modeling (Wu et al., 2021a, Meng et al., 2022), active source seismic monitoring (Gao et al., 2018, 2020; Chi et al., 2020), and DAS monitoring (Li et al., 2020). The first EGS Collab testbed consists of one injection well, one production well, and six monitoring wells, each 50–60 m deep. The project has drilled these wells subhorizontally from the wall of a drift (i.e., a tunnel) into the rock formation, as shown in Figure 1; the injection well is labeled as *I*, and the production well is labeled as *P*. A specialized tool cuts six ring-shaped grooves with sharp edges into the wall of the injection

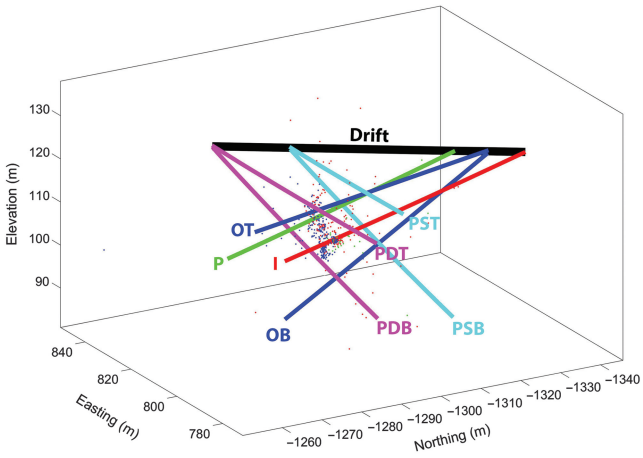

Figure 1. Diagram showing 3D view of boreholes used in EGS Collab testbed 1 at the 1616.67 m (or 4850 ft) depth level of the SURF. The thick black line is the drift, the red line is the injection well, the green line is the production well, the blue lines are referred to as the orthogonal (to the fracture plane) monitoring wells (OB OT), the cyan lines are the parallel shallow monitoring wells (PST and PSB), and the magenta lines are the parallel deep monitoring wells (PDT and PDB). The dots show microseismic events recorded from 22–25 May 2018. The 1.6 km DAS fiber cable is deployed in the six monitoring wells.

well to promote the growth of transverse hydraulic fractures at 1.64 m intervals centered around a fracture notch cut at a measured depth of 50.2 m in the injection well (Fu et al., 2021). Two monitoring wells are orthogonal to these fracture planes and are called the orthogonal bottom (OB) and orthogonal top (OT) wells. The other four monitoring wells are parallel to these fracture planes and are called the parallel shallow top (PST), parallel shallow bottom (PSB), parallel deep top (PDT), and parallel deep bottom (PDB) wells. A DAS system was installed to continuously extend to the six monitoring wells to monitor the hydraulic stimulation experiments in testbed 1 in May and June of 2018 (Li et al., 2020).

The DAS systems, which use fiber-optic cables as densely sampled continuous seismic sensors, have been studied for applications in geothermal settings (Li et al., 2021). Borehole DAS has been extensively used in active source seismic studies using vertical seismic profiling for subsurface imaging, CO_2 monitoring, and geothermal and mineral explorations (Mestayer et al., 2011; Mateeva et al., 2013; Daley et al., 2013, 2016, Li et al., 2015; Wu et al., 2015; Harris et al., 2016; Willis et al., 2016; Zhan et al., 2016; Martuganova et al., 2019; Bellefleur et al., 2020). DAS systems with fiber-optic cables in the conduits have been used to investigate near-surface ambient noise and seismic noise induced by water flow, rain, wind, storm and other human activities at the surface (Dou et al, 2017; Martin et al., 2017; Ajo-Franklin et al., 2019; Shen and Zhu, 2021). However, little research has been conducted on applications of passive DAS ambient noise in boreholes (Chang and Nakata, 2022; Li et al., 2022). Li et al. (2022) demonstrate the feasibility of using borehole DAS ambient noise as a source-free logging tool. They compare DAS-ambient-noise root-mean square (rms) amplitude profiles for the data from the granitic rocks at the Frontier Observatory for Research in Geothermal Energy (FORGE) in Utah with wire-line logging data and find that noisy traces are correlated with possible fracture zones.

We used borehole core photos and core logs to validate the capability of using borehole DAS ambient noise for monitoring hydraulic fracturing at the first testbed of the EGS Collab project. We analyzed the borehole DAS ambient noise data acquired in wells OB and PDB during a 72 h period of fracture stimulation in 22–25 May 2018. This period of time spanned from prior to stimulation 1 to the end of stimulation 3. Stimulation 1 began on 22:06 May 22, 2018 UTC and involved 10.5 min of water injection at a rate of 200 ml/min. Stimulation 2 began on 18:55 23 May 2018 UTC and involved 65.2 min of water injection at a rate of 400 ml/min. Stimulation 3 began on 22:28:00 24 May 2018 UTC and involved injecting water at a rate of 5000 ml/min for 31.7 min until a fracture ruptured through the production well (Schoenball et al., 2020). The fourth and fifth stimulation experiments occurred on 25 May 2018, at 15:32:00 UTC and 20:37:00 UTC, respectively. We computed 72 depth profiles of DAS noise rms depth amplitudes between 00:00:00 22 May and 00:00:00 25 May 2018. We found that the peaks of the DAS noise rms amplitude profiles correspond to fractures and lithologic boundaries after comparing them with the core photos, core logs, and optical televiewer (OTV) logs. We then analyzed the time-lapse changes of the DAS noise rms amplitude profiles between stimulations 2 and 3 and found that the DAS noise rms amplitudes of noisy traces increase, level out, then decrease over time, whereas the DAS noise rms amplitudes of quiet traces do not show significant changes. The time-lapse changes of the DAS noise rms amplitude profiles may correspond to the fracture opening/growth and/or closing during hydraulic stimulation.

DATA AND METHODS

DAS data acquisition and processing

The EGS Collab project installed a DAS system at the first testbed to continuously record DAS data during hydraulic stimulation cycles from 5 April 2018 to 25 June 2018. The DAS system consisted of a Silixa iDAS v.2 interrogator unit that records axial strain-rate data and a 1.6 km optical fiber cable. In each of the six monitoring wells, the project deployed the fiber cable from the well head at the drift to the deepest point (i.e., downgoing) and then back to the drift. The fiber cable extended continuously from one monitoring well to another monitoring well until it traversed all six monitoring wells. The sections of the fiber cable between the monitoring boreholes were left hanging loosely in the drift. The DAS system had a channel spacing of 1 m and a gauge length of 10 m. The sampling frequency varied over time and was either 1 kHz or 10 kHz (Figure 2). Figure 2 shows the DAS sampling frequency during the five stimulation cycles in 22–26 May 2018.

The 1.6 km fiber cable contains approximately 1600 channels (1 m channel spacing). At each channel, the raw DAS data are stored as either 30 s or 60 s records (time series). For this study, we extract the DAS channels along the downgoing fiber cable from the drift to the bottom of each monitoring well. We analyze 72 h of DAS ambient noise data collected between 00:00:00 UTC 22 May 2018 to 00:00:00 UTC 25 May 2018. We decimate the data sampled at 10 kHz to 1 kHz of sampling frequency. For each hour of data, we analyze one minute of DAS ambient noise data and compute DAS noise rms amplitude profiles.

DAS noise rms amplitude profiles

After extracting the DAS ambient noise data from the monitoring wells, we observe that several channels are noisier than the others. We show a 60 s record from well OB between stimulation 2 and stimulation 3 in Figure 3a. To quantify the DAS ambient noise on each trace, we calculate the DAS ambient noise rms amplitude on each channel using

$$A_{\mathrm{rms}} = \sqrt{\frac{1}{N}\sum_{i=1}^{N} y_i^2}, \qquad (1)$$

where A_{rms} is the DAS ambient noise rms amplitude on a channel, y_i is the amplitude at each time step i, and N is the total number of samples in the trace. We calculate the ambient noise rms amplitude on each channel to obtain a noise rms amplitude depth profile. We show such a profile for well OB in Figure 3b. We can see significant noise peaks at depths of 17 m and 29 m whereas there are quiet zones at other depths. To monitor changes in fractures during the hydraulic stimulation cycles, we calculate hourly DAS noise rms amplitude profiles and analyze their time-lapse changes.

RESULTS

Noise rms amplitude profiles

We calculate hourly DAS noise rms amplitude profiles for wells OB and PDB using the DAS ambient noise data acquired in these two wells over a period of 72 h from prior to stimulation 1 to just before stimulation 3 of the hydraulic stimulation cycles in May 2018 (Figure 2).

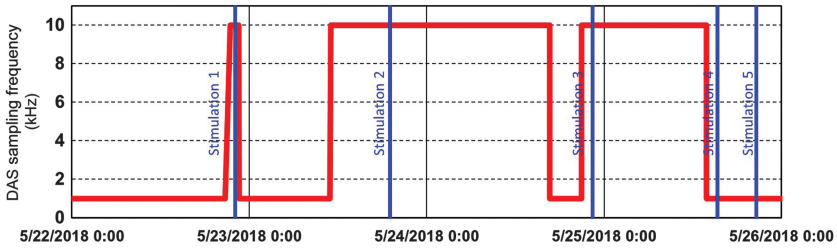

Figure 2. Graph showing the sampling frequency used in DAS data acquisition from 22–26 May 2018. The red line shows the DAS sampling frequency. The blue vertical lines show the onset times of the five hydraulic stimulations in May 2018.

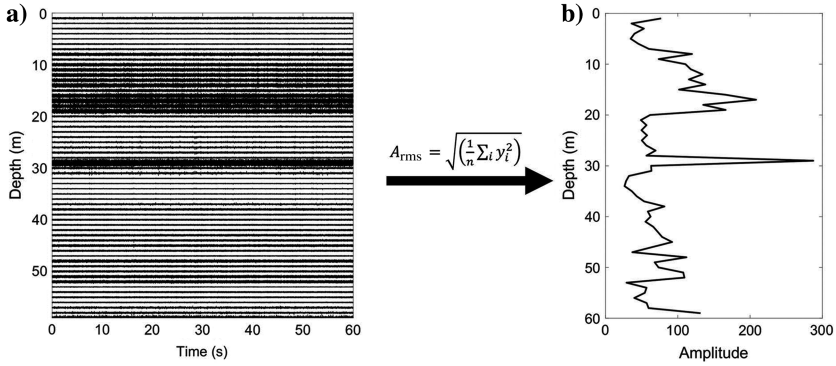

Figure 3. The DAS ambient noise records in well OB. (a) Example 60 s records of DAS ambient noise waveform data recorded in well OB after the onset of stimulation 1 and before the onset of stimulation 2 and (b) a depth profile of the DAS noise rms amplitude.

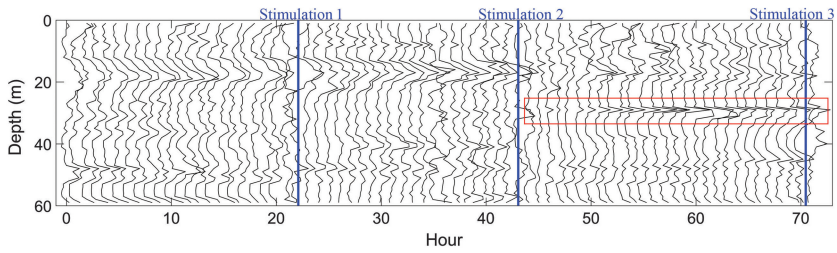

Figure 4. Plot of 72 h depth profiles of DAS noise rms amplitudes in well OB from 22–25 May 2018. For each hour (horizontal axis), we calculate the noise rms amplitude profile using the first 60 s of the DAS ambient noise data recorded within that hour. The blue vertical lines show the onset times of each stimulation cycle. The depth profiles show similar shapes between stimulation cycles but change after the onset of a new stimulation cycle. The red box highlights a peak of the DAS noise rms amplitude profile at the 29 m depth that appears after the onset of stimulation 2. This peak at 29 m varies over time after the onset of stimulation 2.

We calculate one DAS noise rms amplitude profile per hour using the first 60 s of data in the beginning of that hour. Figure 4 shows 72 h DAS noise rms amplitude profiles in well OB. We observe that the DAS noise rms amplitude profiles maintain similar general shapes over time prior to stimulation 1, but they start to vary at the onsets of stimulations 1 and 2. After the onset of stimulation 2, we notice that a noise peak emerges at the 29 m level at approximately hour 46. The amplitude of this noise rms amplitude peak gradually increases over time as shown in the red box in Figure 4. We show 72 h traces of the DAS ambient noise data from a quiet channel (OB-Q25) and a noisy trace (OB-N29) in Figure 5. We observe that, for the quiet channel, the ambient noise amplitudes are similar throughout the 72 h period, whereas the amplitude of the waveform increases steadily after the start of stimulation 2 for the noisy channel.

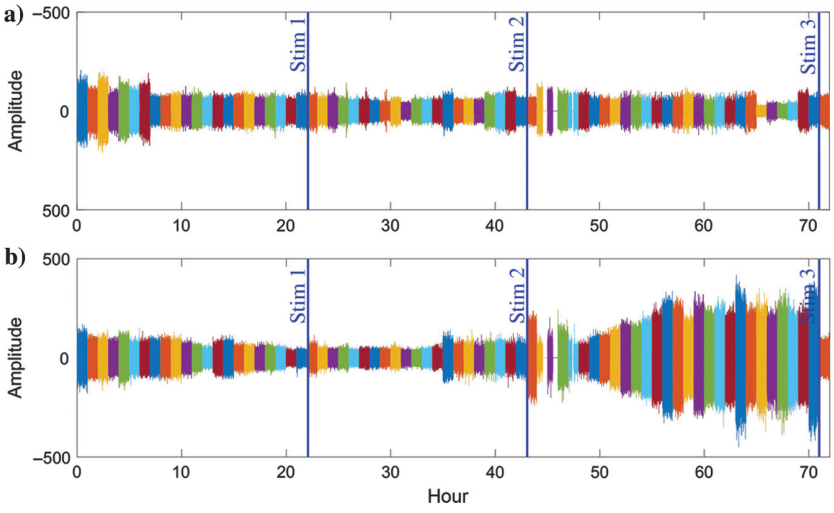

Figure 5. Plot of 72 h (color coded for each hour) time series of data from (a) a quiet trace (OB-Q25) and a (b) noisy trace (OB-N29). The blue vertical lines show the times of the beginning of stimulations 1, 2, and 3. The horizontal axis is time in hours.

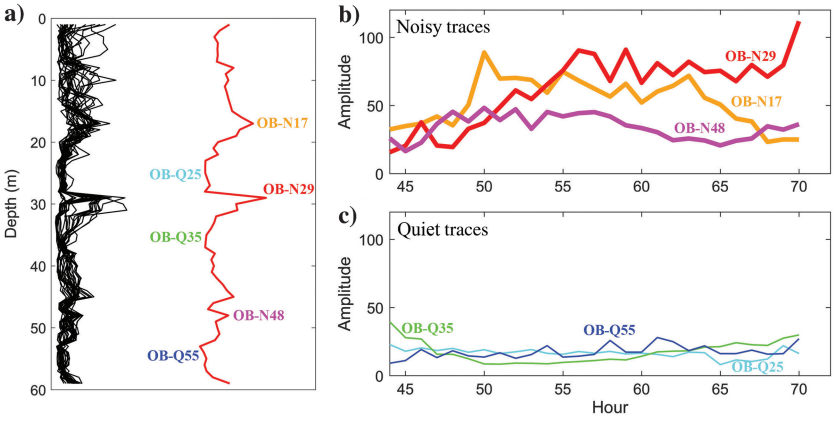

Figure 6. (a) Superimposed hourly DAS noise rms amplitude profiles (the black curves) from well OB for data recorded after stimulation 2 and before stimulation 3 (44–71 h) and the averaged noise rms amplitude profile (the red curve), (b) plot of DAS noise rms amplitude variation over time for noisy channels corresponding to the noise peaks OB-N17 (the orange line), OB-N29 (the red line), and OB-N46 (the magenta line), and (c) plot of DAS noise rms amplitude variation over time for quiet channels corresponding to quiet areas on the noise rms amplitude profile at OB-Q25 (the cyan line), OB-Q35 (the green line), OB-Q55 (the blue line).

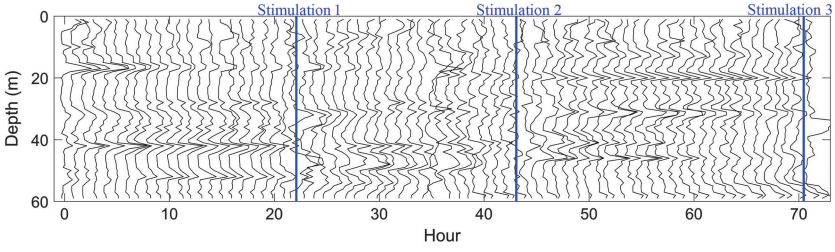

Figure 7. Similar to Figure 4 but for well PDB; 72 h DAS noise rms amplitude profiles in well PDB from 22–25 May 2018.

To further analyze the DAS ambient noise data after stimulation 2, we plot the superimposed hourly noise rms amplitude profiles after stimulation 2 and before stimulation 3 (hour 44–hour 70) as black curves on the left side of Figure 6a. We plot the average of these noise rms amplitude profiles as a red curve on the right side of Figure 6a. The shape of the superimposed curve and the averaged curve show the same general shape with distinct peaks at some depths and quiet regions at other depths. The averaged curve contains distinct noise rms amplitude peaks at 17 m, 29 m, and 48 m labeled as OB-N17, OB-N29, and OB-N48, respectively. The averaged curve also contains quiet depth intervals at approximately 25 m, 35 m, and 55 m labeled as OB-Q25, OB-Q35, and OB-Q55, respectively. We compare time-lapse noise rms amplitudes of noisy channels and those of the quiet channels (Figure 6b and 6c). The DAS noise rms amplitudes of the noisy channels vary over time, but those on the quiet channels show little changes. The amplitude of OB-N29 (the red curve) in Figure 6b starts at approximately 20 in amplitude at hour 44, increases gradually at hour 47, and reaches the maximum of approximately 70 at hour 55 before leveling off. The trends of OB-N17 (the orange curve) and OB-N48 (the magenta curve) in Figure 6b are similar to each other with amplitude increasing, leveling off, and then decreasing. The amplitudes of the quiet traces, OB-Q25 (the cyan line), OB-Q35 (the green line), and OB-Q55 shown in Figure 6c, show slight variations over time, but the general trend remains flat.

We also observe a similar phenomenon for the DAS ambient noise data in PDB. Figure 7 depicts the depth profiles of 72 h of DAS noise rms amplitudes for well PDB. The noise rms amplitude curves also show similar shapes throughout the 72 h period with slight changes after each stimulation cycle. We plot superimposed hourly noise rms amplitude curves from hour 44 to hour 70 as black curves on the left side of Figure 8a and the average of these curves on the right side of

DOI:10.1190/geo2023-0078.1

Figure 8a. The superimposed noise rms amplitude profiles in well PDB are more similar to each other than that those in well OB. The averaged noise rms amplitude profile in well PDB shows several major noise peaks and quiet zones. We label the noise rms amplitude peaks at the 20 m, 31 m, 41 m, and 46 m depths in Figure 8a as PDB-N20, PDB-N31, PDB-N41, and PDB-46, respectively. We plot the time-lapse amplitude variations of these noisy channels after stimulation 2 in Figure 8b. We observe that the noise rms amplitudes of noisy traces follow a general trend of increasing in the few hours after stimulation, leveling off around hour 50, and then slowly decreasing around hour 55–60. We show the noise rms amplitude variation over each hour of the quiet traces in Figure 8b. Compared with the noise rms amplitudes of the noisy traces, the noise rms amplitudes of the quiet traces vary only slightly over time, and the overall trend is flat with no major increases or decreases with time. From Figures 6 and 8, we note that the amplitude reaches a plateau at different times at different locations. The amplitude reaching a plateau at different times could be attributed to the difference in rates of the different fractures opening, reaching a maximum pressure, then closing after injection and shut-off. They also may show the dynamic time-spatial variation of the fracture system.

We hypothesize that fractures around the monitoring wells might cause the noisy zones in the borehole DAS ambient noise data and that the opening/growth/closing of these fractures during hydraulic stimulation would cause the amplitudes of the noisy traces to increase, level off, and decrease after the onset of stimulation 2. Comparing the trends of the time-lapse variations of the DAS noise rms amplitude for well OB (Figure 6b) and well PDB (Figure 8b), we find that the amplitude of the noisy traces in OB and PDB follow a general trend of starting low at the beginning of stimulation 2, increasing during the first 5–10 h after stimulation, and then leveling off or even decreasing. However, for the quiet traces shown in Figures 6c and 8c, we observe only minor variations with time, suggesting that stimulation 2 did not interact with the two monitoring wells at these depths.

To evaluate the frequency spectral components of this noise, we plot the spectral amplitude at each hour for DAS noise traces OB-Q25 (a quiet trace) and OB-N29 (a noisy trace) in Figure 9a and 9b, respectively. The time-frequency spectra of DAS noise traces OB-Q25 and OB-N29 show similar patterns before hour 44. After the onset of stimulation 2, the spectra for OB-N29 exhibit strong amplitudes at all frequencies but the spectra of OB-N25 do not. For a quiet channel (OB-Q25) and a noisy channel (OB-N29), we plot the frequency spectra of each hour of data between stimulation 2 to before stimulation 3 on top of one another in Figure 10. From the Figure 10, we observe that the frequency contents of the quiet and noisy traces are white noise but the amplitude of the noisy traces changes over the duration of stimulation. Li et al. (2022) suggest that trapped waves in low velocity layers caused by fractured media could be an explanation for the higher amplitude ambient noise at some DAS channels. However, other mechanisms also could be possible, such as flow-induced noise, acoustic emissions associated with asperity breakage during stress cycles, and increased local optical noise-caused fiber deformation. To verify whether the DAS noise rms amplitude peaks are caused by fractures around the wellbore, we compare our DAS noise rms amplitude profiles with borehole core photos and OTV logs.

Correlating DAS noise rms amplitude profiles with core photos and OTV logs

We compare our DAS noise rms amplitude profiles with core photos and OTV logs to verify whether the noise rms amplitude

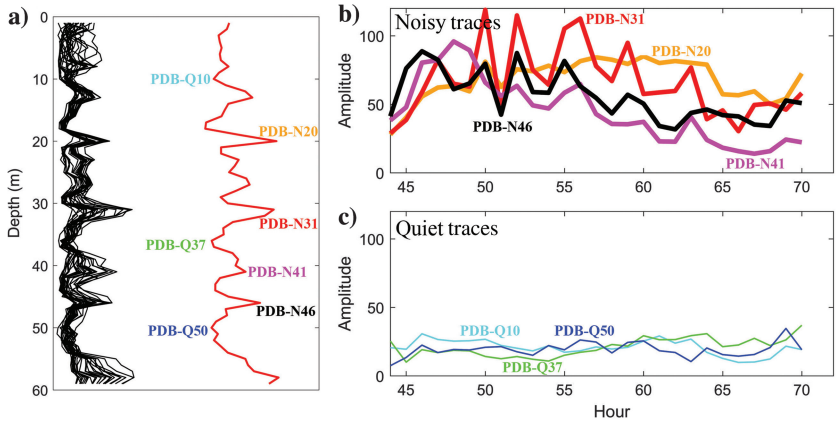

Figure 8. (a) Superimposed noise rms amplitude profiles (the black curves) in well PDB for data recorded after stimulation 1 and before stimulation 2 (44–71 h) and the averaged DAS noise rms amplitude profile (the red line); (b) DAS noise rms amplitude variation over time for noisy channels corresponding to the noise peaks at the four noisy channels PDB-N20 (the orange line), PDB-N31 (the red line), PDB-N41 (the magenta line), and PDB-N46 (the black line); and (c) plot of DAS noise rms amplitude variation over time for quiet channels corresponding to quiet areas on the DAS noise rms amplitude profile at PDB-Q10 (the cyan line), 37 m PDB-Q37 (the green line), and PDB-Q50 (the blue line).

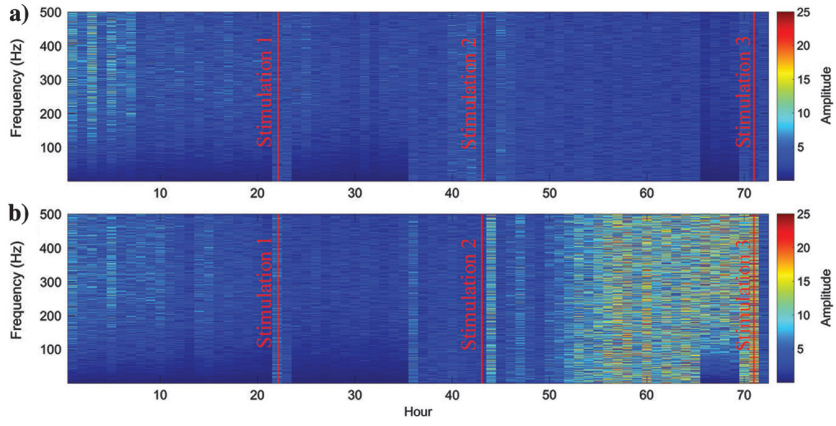

Figure 9. Time-frequency analysis over a 72 h period of (a) OB-Q25 (quiet trace in OB at 25 m depth) and (b) OB-N29 (noisy trace in OB at 29 m depth). The red lines show the times of the onsets of stimulations 1, 2, and 3.

peaks correlate with any fractures observed on core photos and OTV logs. Figure 11 is a comparison between the averaged DAS noise rms amplitude profiles in well OB before stimulation 1 (hour 0–21), between stimulation 1 and stimulation 2 (hour 22–43), and between stimulation 2 and stimulation 3 (hour 44–71) with core photos and OTV logs within the depths with the DAS noise rms amplitudes peaks. These peaks at 17 m, 29 m, and 48 m correspond to the depths where the core contains breaks and fractures or the breaks occurred along mineral intrusions. The noise peak at 17 m (OB-N17) correlates to a break in the core located at a depth of approximately 17.0 m (55.8 ft). This section consists of carbonates and Fe sulfides along with some quartz veins. The peak at 29 m (OB-N29) corresponds to a break in the formation along foliation at a depth of approximately 28.8 m (94.5 ft), mostly having carbonate with iron oxides and iron sulfides. The peak at 48 m (OB-N48) correlates with fractures along strongly undulating weakly bonded mica-rich foliations. We observe two of these fractures at depths of approximately 48.1 m (157.8 ft) and 48.2 m (158 ft).

Figure 12 is a comparison between the averaged DAS noise rms amplitude profiles in well PDB before stimulation 1 (hour 0–21), stimulation 1 and stimulation 2 (hour 22–43), and stimulation 2 and stimulation 3 (hour 44–71), and the core photos. The DAS noise rms amplitude peaks at 20 m, 31 m, and 46 m correlate to areas in the core with fractures or complex geology. The peak at 20 m (PDB-N20) correlates to a fracture in the core at approximately 19.35 m (63.5 ft) depth. This fracture is located along a pyrite and carbonate vein. The peak at the 31 m depth level (PDB-N31) correlates to a section in the core log with complex lithology such as chaotic foliation, highly fractured or brecciated quartz zones, various intrusions of different minerals, and fractures crossing the quartz zones. The bright spot on the OTV log (right-most middle panel) also shows the change in geology of this area. The DAS noise rms amplitude peak at the 46 m depth level (PDB-N46) correlates to breaks in the core along the boundaries of a quartz vein in the schist formation. The depths of these breaks are at 46.0 m (151.2 ft) and 46.3 m (151.8 ft). The OTV log (bottom right panel) also shows this darker-colored quartz vein in the lighter-colored schist formation.

Our results and analyses show that the locations of the major peaks of the DAS noise rms amplitude profiles correlate with the locations of fractures in the formation within wells OB and PDB. Although Li et al. (2022) correlated borehole DAS noise rms amplitude with fracture zones using physical properties from wireline logging data, we use core samples in this study to tie the DAS noise rms amplitude peaks to the actual fractures in the lithology. In addition, we also find that noise rms amplitude peak PDB-N31 correlates with the location of an interpreted fracture plane that intersects well PDB (Fu et al., 2021). Fu et al. (2021)

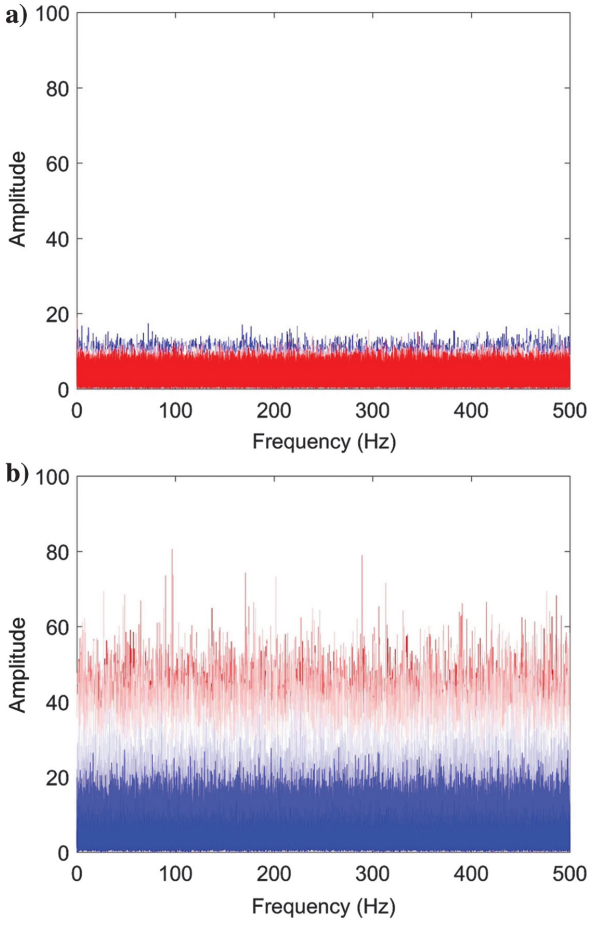

Figure 10. Superimposed frequency spectra of (a) a quiet channel (OB-Q25) and (b) a noisy channel (OB-N29) between stimulation 2 to stimulation 3. The cooler colors show the spectra for 60 s for the data at the start of stimulation and the warmer colors show the spectra immediately before stimulation 2.

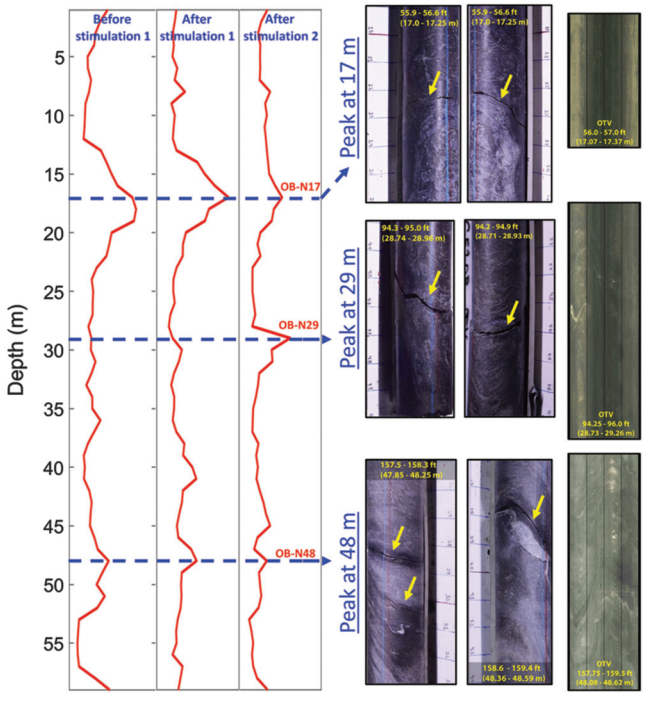

Figure 11. Comparing peaks in the DAS noise rms amplitude profiles in well OB before stimulation 1, after stimulation 1, and after stimulation 2 with core photos corresponding to depths of 17 m, 29 m, and 49 m. We observe that the locations of the noise rms amplitude peaks correspond to open fractures (29 m) and breaks along mineral intrusion boundaries (17 m and 29 m) shown on the core photos. The yellow arrows point to locations of fractures on the core photos.

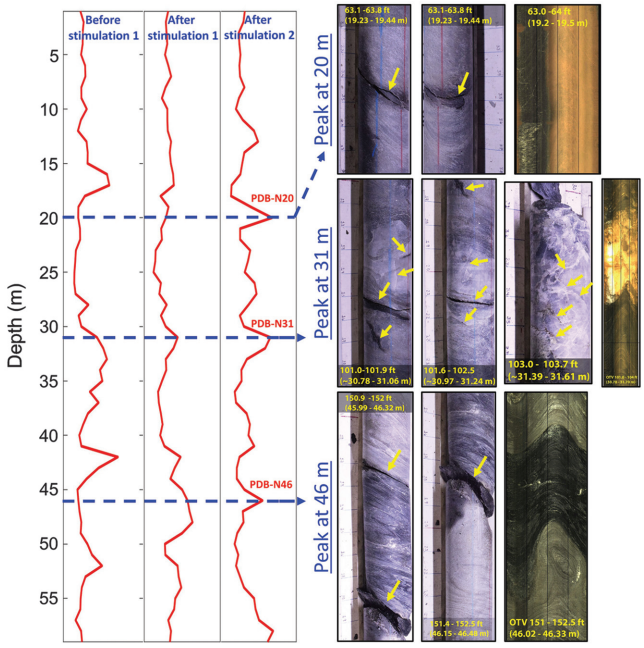

Figure 12. Comparing peaks in the DAS noise rms amplitude profiles in well PDB before stimulation 1, after stimulation 1, and after stimulation 2 with core photos corresponding to depths of 20 m, 31 m, and 46 m. We observe that the locations of the DAS noise rms amplitude peaks correspond to fractured crystalline rock (31 m) and breaks along lithologic boundaries (46 m) shown on the core photos.

fit planes to microseismic locations caused by the fracture stimulation cycles in May 2018 and obtain interpreted fracture planes. One of the fracture planes, fracture E-S, is found to intersect the well at a depth of 32 m. This intersection point of 32 m is close to the location of DAS noise rms amplitude peak PDB-N31 located at a depth of 31 m. In addition, distributed temperature sensing measurements from well PDB show a temperature anomaly at approximately 33 m depth (Fu et al., 2021). Fracture modeling using the temperature data indicates that a fracture crosses well PDB at approximately this depth (Wu et al., 2021b). Our results show that borehole DAS ambient noise analysis can locate fracture zones in the borehole and monitor changes during hydraulic fracture stimulation.

CONCLUSION

We have analyzed borehole DAS ambient noise data recorded during hydraulic fracture stimulation at the first EGS Collab testbed and found that the DAS noise rms amplitude profiles contain distinct peaks at certain depths. We have compared the DAS noise rms amplitude profiles with core photos, core logs, and OTV logs and verified that the peaks in the DAS noise rms amplitude profiles correlate with the locations of fractures, complex lithology, or lithologic boundaries. In addition, we have found that the DAS noise rms amplitudes of the noisy channels vary with time after stimulation 2, following a general trend of increasing amplitude after the stimulation onset, leveling off after several hours, then decreasing. We attribute the changes of the DAS noise rms amplitudes of these noisy channels to the opening/growth of fractures at the beginning of hydraulic stimulation, keeping these fractures open during stimulation, and gradual closing of the fractures after the stimulation. Our results show that borehole DAS ambient noise data could be used to not only locate and detect fractures but also to monitor these fractures during hydraulic stimulation in EGS reservoirs.

ACKNOWLEDGMENTS

This material was based upon work supported by the U.S. Department of Energy (DOE), Office of Energy Efficiency and Renewable Energy (EERE), Office of Technology Development, Geothermal Technologies Office (GTO), under Contract No. 89233218CNA000001 to Los Alamos National Laboratory (LANL). LANL is operated by Triad National Security, LLC, for the National Nuclear Security Administration (NNSA) of U.S. DOE. The United States Government retains and the publisher, by accepting the article for publication, acknowledges that the United States Government retains a nonexclusive, paid-up, irrevocable, world-wide license to publish or reproduce the published form of this manuscript, or allow others to do so, for United States Government purposes. The research supporting this work took place in whole or in part at the Sanford Underground Research Facility in Lead, South Dakota. The assistance of the Sanford Underground Research Facility and its personnel in providing physical access and general logistical and technical support is acknowledged. Y. Zheng and Y. Li were supported by DOE GTO through the University of Houston under Contract No. DE-EE0008764. We thank T. Zhu, two anonymous reviewers, and the editors for their valuable comments.

DATA AND MATERIALS AVAILABILITY

Data associated with this research are available and can be obtained by contacting the corresponding author.

REFERENCES

Ajo-Franklin, J. B., S. Dou, N. J. Lindsey, I. Monga, C. Tracy, M. Robertson, V. Rodriguez Tribaldos, C. Ulrich, B. Freifeld, T. Daley, and X. Li, 2019, Distributed acoustic sensing using dark fiber for near-surface characterization and broadband seismic event detection: Scientific Reports, **9**, 1328, doi: 10.1038/s41598-018-36675-8.

Bellefleur, G., E. Schetselaar, D. Wade, D. White, R. Enkin, and D. R. Schmitt, 2020, Vertical seismic profiling using distributed acoustic sensing with scatter-enhanced fibre-optic cable at the Cu–Au New Afton porphyry deposit, British Columbia, Canada: Geophysical Prospecting, **68**, 313–333, doi: 10.1111/1365-2478.12828.

Chang, H., and N. Nakata, 2022, Investigation of time-lapse changes with DAS borehole data at the brady geothermal field using deconvolution interferometry: Remote Sensing, **14**, 185, doi: 10.3390/rs14010185.

Chen, Y.L. Huang, and , EGS Collab Team, 2019, Optimal design of 3D borehole seismic arrays for microearthquake monitoring in anisotropic media during stimulations in the EGS collab project: Geothermics, **79**, 61–66, doi: 10.1016/j.geothermics.2019.01.009.

Chi, B., L. Huang, K. Gao, J. Ajo-Franklin, and T. J. Kneafsey, 2020, Anisotropic imaging of created fractures in EGS Collab experiments using CASSM data: Proceedings of the 45th Workshop on Geothermal Reservoir Engineering, 6.

Daley, T. M., B. M. Freifeld, J. Ajo-Franklin, S. Dou, R. Pevzner, V. Shulakova, S. Kashikar, D. E. Miller, J. Goetz, J. Henninges, and S. Lueth, 2013, Field testing of fiber-optic distributed acoustic sensing (DAS) for subsurface seismic monitoring: The Leading Edge, **32**, 699–706, doi: 10.1190/tle32060699.1.

Daley, T. M., D. E. Miller, K. Dodds, P. Cook, and B. M. Freifeld, 2016, Field testing of modular borehole monitoring with simultaneous distributed acoustic sensing and geophone vertical seismic profiles at Citronelle, Alabama: Geophysical Prospecting, **64**, 1318–1334, doi: 10.1111/1365-2478.12324.

Dobson, P., T. J. Kneafsey, D. Blankenship, C. Valladao, J. Morris, H. Knox, P. Schwering, M. White, T. Doe, W. Roggenthen, and E. Mattson, 2017, An introduction to the EGS Collab Project: GRC Transactions, **41**, 837–849.

Dou, S., N. Lindsey, A. M. Wagner, T. M. Daley, B. Freifeld, M. Robertson, J. Peterson, C. Ulrich, E. R. Martin, and J. B. Ajo-Franklin, 2017, Distributed acoustic sensing for seismic monitoring of the near surface: A traffic-noise interferometry case study: Scientific Reports, **7**, 11620, doi: 10.1038/s41598-017-11986-4.

Fu, P., M. Schoenball, J. B. Ajo-Franklin, C. Chai, M. Maceira, J. P. Morris, H. Wu, H. Knox, P. C. Schwering, M. D. White, and J. A. Burghardt, 2021, Close observation of hydraulic fracturing at EGS Collab Experiment 1: Fracture trajectory, microseismic interpretations, and the role of natural fractures: Journal of Geophysical Research: Solid Earth, **126**, e2020JB020840, doi: 10.1029/2020JB020840.

Gao, K., L. Huang, B. Chi, and J. Ajo-Franklin, 2018, Imaging the fracture zone using continuous active source seismic monitoring for the EGS Collab project: A synthetic study: Proceedings of the 43rd Workshop on Geothermal Reservoir Engineering.

Gao, K., L. Huang, H. Knox, P. C. Schwering, C. Hoots, J. Ajo-Franklin, and T. Kneafsey, 2020, Anisotropic elastic properties of the first EGS Collab testbed revealed from the campaign cross-borehole seismic data: Proceedings 45th Workshop on Geothermal Reservoir Engineering, Stanford University, SGPTR-216, preprint, https://pangea.stanford.edu/ERE/db/GeoConf/papers/SGW/2020/Gao1.pdf (accessed January 2022).

Harris, K., D. White, D. Melanson, C. Samson, and T. M. Daley, 2016, Feasibility of time-lapse VSP monitoring at the Aquistore CO_2 storage site using a distributed acoustic sensing system: International Journal of Greenhouse Gas Control, **50**, 248–260, doi: 10.1016/j.ijggc.2016.04.016.

Kneafsey, T. J., D. Blankenship, P. F. Dobson, J. P. Morris, M. D. White, P. Fu, P. C. Schwering, J. B. Ajo-Franklin, L. Huang, M. Schoenball, and T. C. Johnson, 2020, The EGS collab project: Learnings from Experiment 1: Proceedings of the 45th Workshop on Geothermal Reservoir Engineering, Stanford University, 10–12.

Kneafsey, T. J., D. Blankenship, H. A. Knox, T. C. Johnson, J. B. Ajo-Franklin, P. C. Schwering, P. F. Dobson, J. P. Morris, M. D. White, R. Podgorney, and W. Roggenthen, 2019, EGS Collab project: Status and progress: Proceedings of the 44th Workshop on Geothermal Reservoir Engineering, Stanford University.

Kneafsey, T. J., P. Dobson, D. Blankenship, J. Morris, H. Knox, P. Schwering, M. White, T. Doe, W. Roggenthen, E. Mattson, and R. Podgorney, 2018, An overview of the EGS Collab project: field validation of coupled process modeling of fracturing and fluid flow at the Sanford Underground Research Facility, Lead, SD: Proceedings of the 43rd Workshop on Geothermal Reservoir Engineering.

Lambert, C. E., 2022, Beneath your feet and in your place: Multi-scalar imaginaries of energy, place, and local geothermal development: Energy Research & Social Science, **94**, 102856, doi: 10.1016/j.erss.2022.102856.

Li, D., L. Huang, B. Chi, J. Ajo-Franklin, V. R. Tribaldos, and M. Schoenball, 2020, Distributed acoustic sensing monitoring at the first EGS Collab testbeds: Proceedings of the 45th Workshop on Geothermal Reservoir Engineering, Stanford University.

Li, D., L. Huang, Y. Zheng, Y. Li, P. Wannamaker, and J. Moore, 2022, Feasibility of source-free DAS logging for next-generation borehole imaging: Scientific Reports, **12**, 11910, doi: 10.1038/s41598-022-16027-3.

Li, Y. and M. Karrenbach and J. Ajo-Franklin, eds., 2021, Distributed acoustic sensing in geophysics: Methods and applications: John Wiley & Sons.

Li, Y., H. Wu, W. Wong, B. Hewett, Z. Liu, A. Mateeva, and J. Lopez, 2015, Velocity analysis and update with 3D DAS-VSP to improve borehole/surface seismic images: 85th Annual International Meeting, SEG, Expanded Abstracts, 5285–5289, doi: 10.1190/segam2015-5864923.1.

Martin, E. R., C. M. Castillo, S. Cole, P. S. Sawasdee, S. Yuan, R. Clapp, M. Karrenbach, and B. L. Biondi, 2017, Seismic monitoring leveraging existing telecom infrastructure at the SDASA: Active, passive, and ambient-noise analysis: The Leading Edge, **36**, 1025–1031, doi: 10.1190/tle36121025.1.

Martuganova, E., J. Henninges, M. Stiller, K. Bauer, B. Norden, C. Krawczyk, and E. Huenges, 2019, DAS-VSP measurements using wireline logging cable at the Groß Schönebeck geothermal research site, NE German Basin: 81st Annual International Conference and Exhibition, EAGE, Extended Abstracts, doi: 10.3997/2214-4609.201901246.

Mateeva, A., J. Lopez, J. Mestayer, P. Wills, B. Cox, D. Kiyashchenko, Z. Yang, W. Berlang, R. Detomo, and S. Grandi, 2013: Distributed acoustic sensing for reservoir monitoring with VSP: The Leading Edge, **32**, 1278–1283, doi: 10.1190/tle32101278.1.

Meng, M., L. P. Frash, W. Li, N. J. Welch, J. W. Carey, J. Morris, G. Neupane, C. Ulrich, and T. Kneafsey, 2022, Hydro-mechanical measurements of sheared crystalline rock fractures with applications for EGS Collab Experiments 1 and 2: Journal of Geophysical Research: Solid Earth, **127**, e2021JB023000, doi: 10.1029/2021JB023000.

Mestayer, J., B. Cox, P. Wills, D. Kiyashchenko, J. Lopez, M. Costello, S. Bourne, G. Ugueto, R. Lupton, G. Solano, and D. Hill, 2011, Field trials of distributed acoustic sensing for geophysical monitoring: 81st Annual International Meeting, SEG, Expanded Abstracts, 4253–4257, doi: 10.1190/1.3628095.

Schoenball, M., J. B. Ajo-Franklin, D. Blankenship, C. Chai, A. Chakravarty, P. Dobson, C. Hopp, T. Kneafsey, H. A. Knox, M. Maceira, and M. C. Robertson, 2020, Creation of a mixed-mode fracture network at mesoscale through hydraulic fracturing and shear stimulation: Journal of Geophysical Research: Solid Earth, **125**, e2020JB019807, doi: 10.1029/2020JB019807.

Shen, J., and T. Zhu, 2021, Characterizing urban seismic noise recorded by distributed acoustic sensing array: First International Meeting for Applied Geoscience & Energy, SEG, Expanded Abstracts, 3215–3219, doi: 10.1190/segam2021-3583704.1.

Willis, M. E., C. Erdemir, A. Ellmauthaler, O. Barrios, and D. Barfoot, 2016, Comparing DAS and geophone zero-offset VSP data sets side-by-side: CSEG Recorder, **41**, 22–26.

Wu, H., P. Fu, Z. Frone, M. D. White, J. B. Ajo-Franklin, J. P. Morris, H. A. Knox, P. C. Schwering, C. E. Strickland, B. Q. Roberts, and V. R. Vermeul, 2021b, Modeling heat transport processes in enhanced geothermal systems: A validation study from EGS Collab Experiment 1: Geothermics, **97**, 102254, doi: 10.1016/j.geothermics.2021.102254.

Wu, H., P. Fu, J. P. Morris, E. D. Mattson, G. Neupane, M. M. Smith, A. J. Hawkins, Y. Zhang, T. Kneafsey, and , EGS Collab Team, 2021a, Characterization of flow and transport in a fracture network at the EGS Collab field experiment through stochastic modeling of tracer recovery: Journal of Hydrology, **593**, 125888, doi: 10.1016/j.jhydrol.2020.125888.

Wu, H., W. Wong, Z. Yang, P. Wills, J. Lopez, Y. Li, B. Blonk, B. Hewett, and A. Mateeva, 2015, Dual-well 3D vertical seismic profile enabled by distributed acoustic sensing in deep water Gulf of Mexico: Interpretation, **3**, no. 3, SW11–SW25, doi: 10.1190/INT-2014-0248.1.

Zhan, G., Q. Li, J. Nahm, J. Kommedal, and J. Konkler, 2016, Field trials of distributed acoustic sensing for reservoir delineation with VSP: CSEG Recorder, **41**, 34–37.

Biographies and photographs of the authors are not available.

DOI:10.1190/geo2023-0078.1